Science Advances
AAAS

advances.sciencemag.org/cgi/content/full/6/26/eaaz0495/DC1

Supplementary Materials for

Carbon nanocarriers deliver siRNA to intact plant cells for efficient gene knockdown

Gozde S. Demirer, Huan Zhang, Natalie S. Goh, Rebecca L. Pinals, Roger Chang, Markita P. Landry*

*Corresponding author. Email: landry@berkeley.edu

Published 24 June 2020, *Sci. Adv.* **6**, eaaz0495 (2020)
DOI: 10.1126/sciadv.aaz0495

The PDF file includes:

Other Supplementary Material for this manuscript includes the following:

(available at advances.sciencemag.org/cgi/content/full/6/26/eaaz0495/DC1)

Thermodynamic analysis of RNA desorption and hybridization

Herein, we perform a thermodynamic analysis to model whether siRNA sense and antisense complementary strands desorb from the SWNT surface and hybridize to each other in either the intracellular or extracellular environment (**Fig. 3**). In both cases, it is assumed that the single-stranded RNA (ssRNA) desorption from the SWNT surface is the first step, followed by hybridization of free ssRNA to form double-stranded RNA (dsRNA): nucleic acid adsorption to SWNTs is through π-π interactions and H-bonding to neighboring strands, therefore, in order to hybridize and form Watson-Crick base-pairing H-bonds, the ssRNA strands first must desorb from the SWNT surface.

Extracellular thermodynamics analysis

Calculation for ssRNA desorption from SWNT:

In this analysis, we use energy values for adsorption of individual nucleobases to SWNTs from Johnson *et al.* (*47*) (Supplementary Table 1) to calculate the total desorption energy of each ssRNA sequence used in this study (Supplementary Table 2). Johnson *et al.* (*47*) use solvent-explicit, all-atom molecular dynamics (MD) simulations for 21-nucleotide hetero- and homo-polymers adsorbing to SWNTs. Note that these energies are in close agreement with Das et al. (*48*), calculated from density functional theory (DFT) and experiment.

Supplementary Table 1: Adsorption energy of each nucleotide to SWNTs *(47)*

Base	Energy [kcal/mol]
A	-13.84
G	-14.99
C	-11.07

T = U	-12.68

Using these adsorption energies, we calculate the average desorption energy of ssRNA from the SWNT surface to be +275.3 kcal/mol ± 11.25, which we then multiply by 2 ssRNA strands to have **+550.6 kcal/mol** for both siRNA sense and antisense desorption from SWNTs (Supplementary Table 2).

Supplementary Table 2: ssRNA-SWNT desorption energy and RNA hybridization energy for each ssRNA sequence

Sequence Name	Sequence	Desorption Energy [kcal/mol]	Hybridization Energy [kcal/mol]
a-antisense	UUC CGU AUG UUG CAU CAC CTT	267.1	-39.22
a-sense	GGU GAU GCA ACA UAC GGA ATT	283.4	-39.10
b-antisense	GGG UGA AGG UGA UGC AAC ATT	288.5	-39.67
b-sense	UGU UGC AUC ACC UUC ACC CTT	261.5	-39.80
NT-antisense	GUA UCU CUU CAU AGC CUU ATT	267.5	-33.76
NT-sense	UAA GGC UAU GAA GAG AUA CTT	283.9	-33.89
	Average	**275.3**	**-39.37**
	Standard deviation	11.25	0.3743

Calculation for ssRNA to dsRNA hybridization:

ssRNA hybridization next occurs in solution. We use the OligoAnalyzer tool through Integrated DNA Technologies, Inc., with the following assumed ion and ssRNA concentrations: [Na^+] = 10 mM, [Mg^{2+}] = 0.1mM, and [ssRNA] = 0.25 μM. We calculate the hybridization energy for each ssRNA sequence used in this study, and the average hybridization energy is **-39.37 kcal/mol** ± 0.3743 (Supplementary Table 2). Therefore, the overall free energy change under extracellular conditions is:

$$\Delta G_{extracell} = \Delta G_{ssRNA,des} + \Delta G_{hyb} = \left(+550.6\frac{kcal}{mol}\right) + \left(-39.37\frac{kcal}{mol}\right) = +\mathbf{511.2}\,\boldsymbol{\frac{kcal}{mol}}$$

Based on this positive (unfavorable) free energy change, our analysis demonstrates that it is unlikely for ssRNA desorption and hybridization to take place spontaneously in the extracellular environment when both complementary ssRNA strands are initially adsorbed on SWNTs.

Intracellular thermodynamics analysis

The intracellular environment is crowded with biomolecules, is highly dynamic, and intracellular components of the cell cytoplasm such as proteins and lipids are known to bind to SWNTs (*49*). Accordingly, once inside the cell, cytoplasmic biomolecules will likely adsorb on SWNTs, as observed by SWNT solvatochromic shifts (**Fig. S5**) (*50*), and replace the nucleic acids originally on the SWNT surface *(51)*. Therefore, we hypothesize that inside the cell, ssRNA desorption and hybridization are likely to take place because the high free energy of "bare" SWNTs is avoided by direct biomolecule replacement, hence making this process thermodynamically favorable under cytoplasmic conditions as calculated below (**Fig. 3**). We assume that the same ssRNA desorption energies apply, but now this unfavorable ssRNA desorption is countered by favorable protein adsorption to the SWNT surface.

<u>Calculation for protein adsorption energy to SWNTs:</u>

We assume that the ssRNA desorption and protein adsorption steps take place independently, as shown to be likely from experiment *(51)*. Shen *et al.* (*52*) use MD simulations to model the adsorption of human serum albumin (HSA) helices on different chirality SWNTs with water as the solvent and calculate an average protein adsorption energy of -14.51 kcal/mol ± 1.858 per amino acid. Similarly, DFT calculations have

reported protein adsorption to carbon nanotubes with an average energy of ~ -10 kcal/mol per amino acid (*53*, *54*). We assume **-10 kcal/mol** binding energy per amino acid.

To calculate how many amino acids replace each pre-adsorbed ssRNA strand on the SWNT surface, we make the following contact area estimations. First, nucleic acids have been shown to form helices wrapping around SWNTs above a length of ~12 nucleic acids *(55)*. Since these ssRNA strands are 21-mers, we assume helix morphology. RNA is known to adopt A-form helices, in which there are 25 Å per helical turn and ~11 nucleotides per helical turn, therefore 2.27 Å per nucleotide *(56)*. For the 21-mer ssRNA, this is 47.67 Å "helix length" *L* along the SWCNT. Estimating that the nucleotides occupy the entire space between helically wrapped strands, this allows the surface area calculation: $SA_{cyl} = 2\pi rL$, where r = 0.5 nm on average for these SWNTs, therefore SA_{cyl} = 14.98 nm^2 or **1,498 Å²**. This contact area calculation is within a reasonable order of magnitude, in comparison to an MD simulation of helix-forming $(GT)_{15}$ (30-mer) ssDNA on SWNTs occupying 2,400 $Å^2$, or 80 $Å^2$ per nucleotide (versus 71.31 $Å^2$ per ssRNA as calculated above). Next, for protein contact area, we use beta sheet dimensions as a proxy of protein adsorption to SWNTs. In beta sheets, there are 3.25 Å per amino acid for *X* amino acids, or 3.25**X* Å "lengthwise" on the SWNT. The "width" of the protein along the SWNT can be approximated as twice the R-group width for beta sheet geometry. Assuming aromatic R-group amino acids (Tyr, Phe, Trp) interact with SWNTs *(53, 54)* and calculating dimensions based on bond lengths, the average R-group dimension is 5.69 Å, or W = 2*5.69 = 11.38 Å. Then, contact area $SA_{rect} = L*W$ = 36.99**X* $Å^2$. Comparing the ssRNA to protein estimated surface areas, we see that **40.5 amino acids** replace one 21-mer ssRNA on the SWNT surface.

Accordingly, for 40.5 amino acids and -10 kcal/mol per amino acid, we obtain -405 kcal/mol for an average protein adsorption energy to SWNTs. Note that this energy is within a reasonable order of magnitude, as HSA adsorption on carboxylated SWNTs is ~ -500 kcal/mol via MD simulation (*57*). Moreover, the median number of amino acids per protein in *A. thaliana* is 356 amino acids (*58*), and assuming ~10% amino acids participate in protein adsorption gives -356 kcal/mol. Finally, multiplying by 2 SWNTs, we have **-810 kcal/mol** for protein adsorption to the SWNT surface. Therefore, the overall change in free energy in intracellular conditions is:

$$\Delta G_{intracell} = \Delta G_{ssRNA,des} + \Delta G_{prot,ads} + \Delta G_{hyb}$$

$$= \left(+550.6\frac{kcal}{mol}\right) + \left(-810\frac{kcal}{mol}\right) + \left(-39.37\frac{kcal}{mol}\right) = \mathbf{-298.8\frac{kcal}{mol}}$$

Our analysis shows that this overall free energy change is negative inside plant cells, which demonstrates that desorption from the SWNT surface and subsequent hybridization of complementary ssRNA sequences are favorable and spontaneous in intracellular conditions, recapitulating our experimental results.

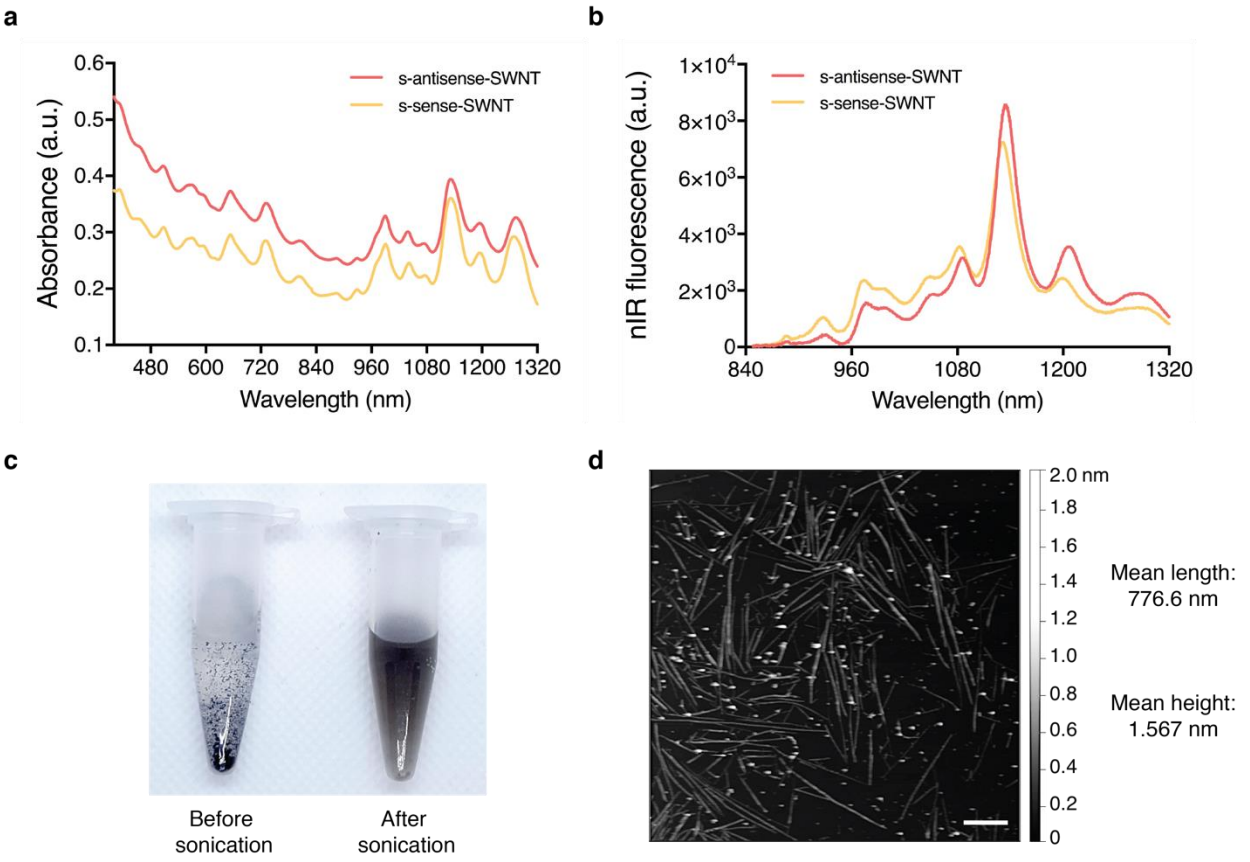

Supplementary Fig. 1. Non-targeting s-RNA-SWNT suspension characterization and AFM imaging. a Absorbance spectra of s-antisense-SWNT and s-sense-SWNT suspensions. **b** Near-infrared (nIR) fluorescence spectra of s-antisense-SWNT and s-sense-SWNT suspensions. **c** Photo on the left showing RNA SWNT mixture before probe-tip sonication where unsuspended SWNTs aggregate due to van der Waals and hydrophobic interactions between SWNTs, and photo on the right showing homogenous dark-colored individually suspended RNA-SWNT solution that is colloidally stable following probe-tip sonication. Photo credit: Gozde S. Demirer, UC Berkeley. **d** Representative atomic force microscopy (AFM) image of an ssRNA-SWNT suspension. Scale bar, 100 nm. Mean length of RNA-SWNTs is 776.6 nm (st. dev. 163 nm) and mean height is 1.567 nm (st. dev. 0.38 nm) for N = 25 SWNTs.

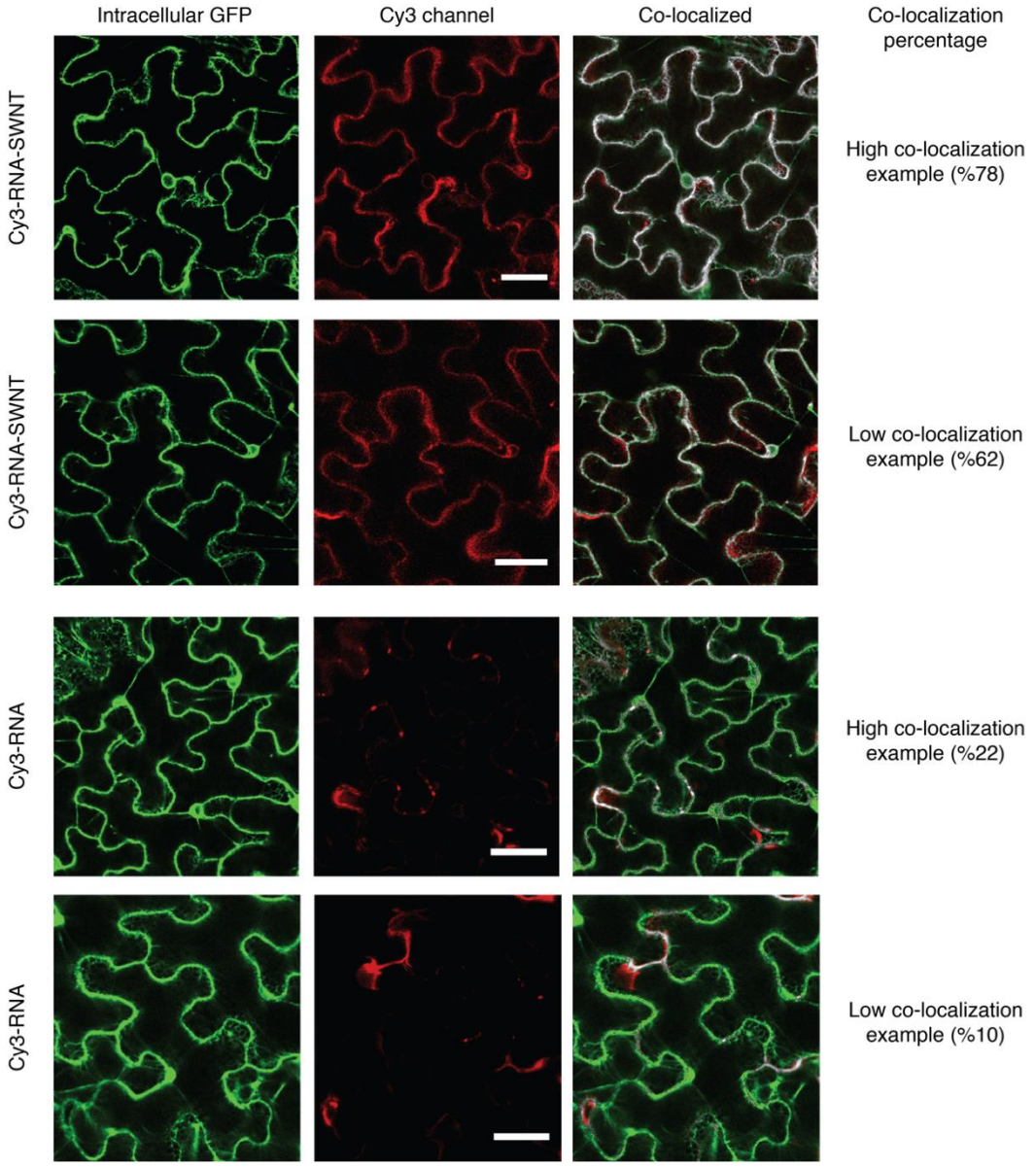

Supplementary Fig. 2. Internalization of Cy3-RNA-SWNT and Cy3-RNA into mGFP5 *Nicotiana benthamiana* leaves assessed with confocal microscopy and co-localization analysis. Top two rows: Cy3-RNA-SWNT infiltrated *Nb* leaf images showing examples of high (78%) and low (62%) co-localization percentages of intracellular GFP with Cy3-RNA-SWNT fluorescence. Bottom two rows: Free Cy3-RNA infiltrated *Nb* leaf images showing examples of high (22%) and low (10%) co-localization percentage of intracellular GFP with free Cy3-RNA fluorescence. Scale bars are 40 µm.

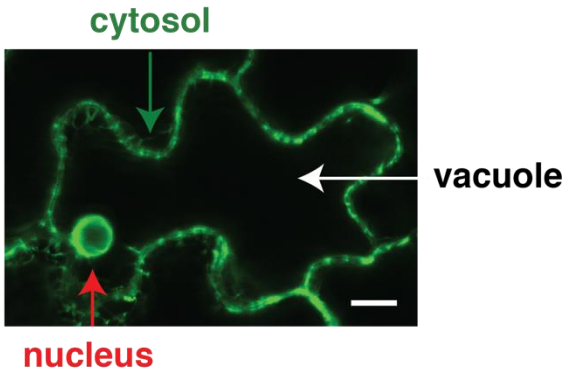

Supplementary Fig. 3. Subcellular areas in GFP *Nicotiana benthamiana* leaf cells. Green arrow shows the cytosol pushed back to the cell membrane due to the presence of the large central plant cell vacuole. Red arrow marks the nucleus and white arrow marks the vacuole in a leaf epidermal cell imaged with confocal microscopy. Scale bar: 20 µm.

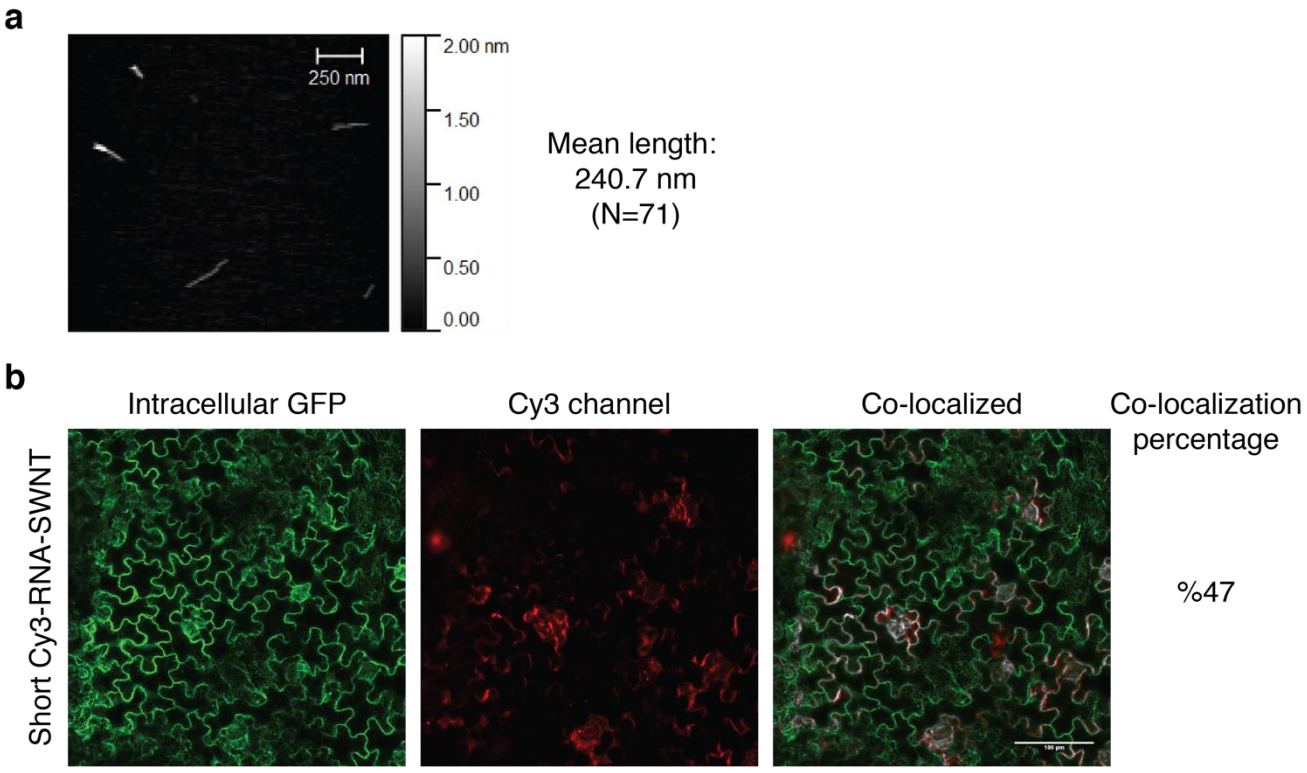

Supplementary Fig. 4. Short Cy3-RNA-SWNTs and their internalization efficiency analysis. a Representative AFM image showing shortened SWNTs with an average length of ~250 nm. **b** Representative short Cy3-RNA-SWNT infiltrated *Nb* leaf confocal image showing 47% co-localization percentage of intracellular GFP with Cy3-RNA-SWNT fluorescence.

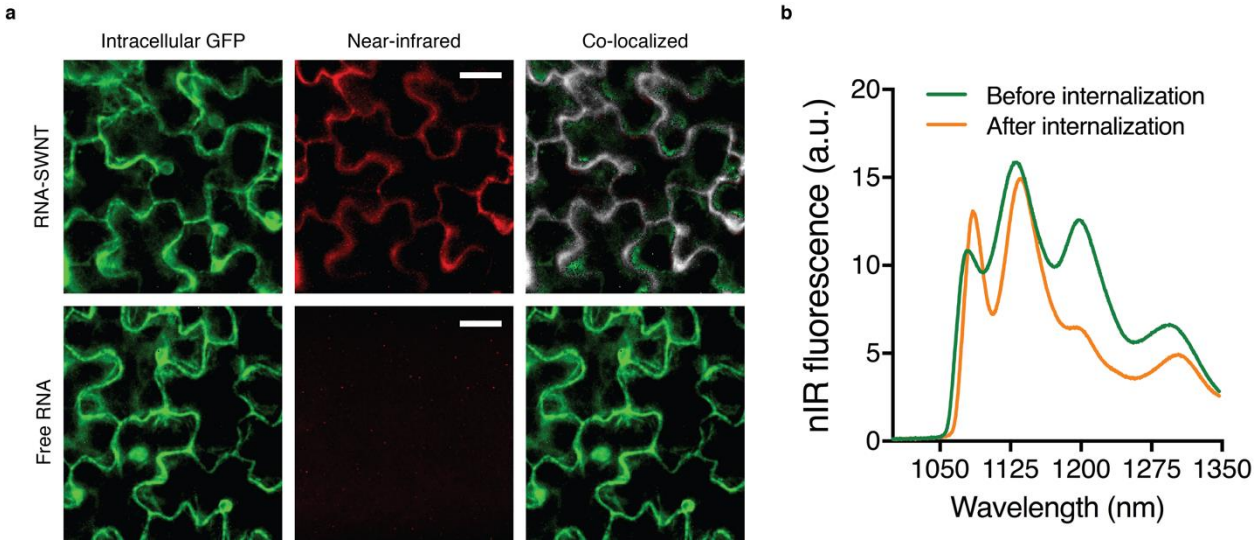

Supplementary Fig. 5. nIR imaging shows internalization of RNA-SWNT suspensions into mGFP5 *Nicotiana benthamiana* leaves. a Top row: RNA-SWNT infiltrated *Nb* leaf images showing high co-localization efficiency of intracellular GFP with intrinsic nIR SWNT fluorescence. Bottom row: Free RNA infiltrated *Nb* leaf images showing no co-localization of free RNA inside cells. Scale bars are 20 µm. **b** nIR fluorescence spectra of RNA-SWNTs before and after internalization into leaf cells. Spectra were obtained with a 1050-nm long pass filter to avoid the autofluorescence of chlorophyll from leaves.

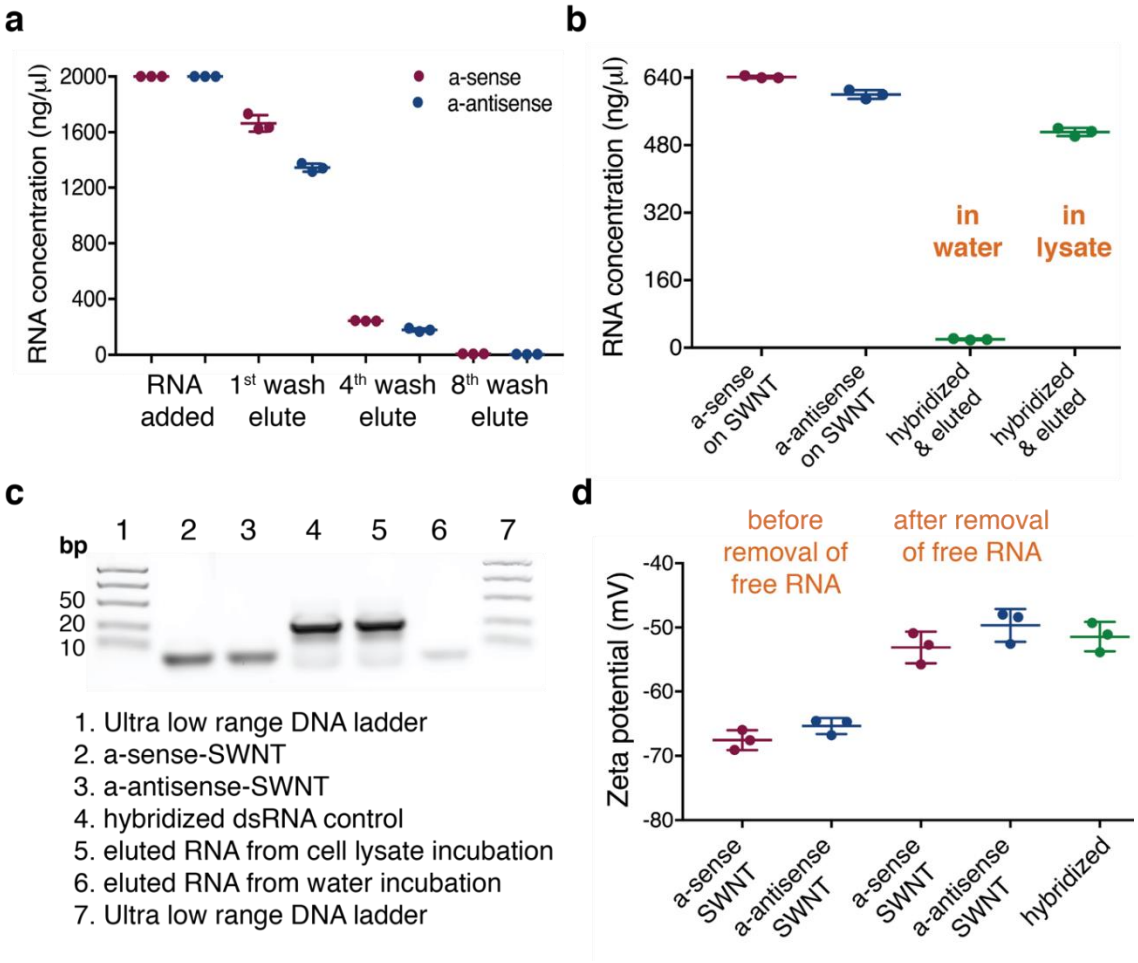

Supplementary Fig. 6. Characterization of dsRNA hybridization and desorption. a a-sense and a-antisense RNA amount added to suspend SWNTs, RNA concentration in the 1st, 4th and 8th flow-through solutions after centrifugation with 100K spin filters to remove free RNA after suspension with SWNTs (RNA concentration is calculated via absorbance measurements at 260 nm). **b** RNA amount on suspended SWNTs (calculated via total RNA added – free RNA removed via spin filtration), dsRNA eluted after hybridization in water and in cell lysate conditions. **c** 4% agarose gel showing eluted RNA from cell lysate and water incubations, 97% double stranded RNA is eluted from the cell lysate incubation and 19% of single stranded RNA is eluted from the water incubation sample. **d** Zeta potential measurements for a-sense-SWNT and a-antisense-SWNT suspensions before and after the removal of free RNA, and after mixing a-sense-SWNT and a-antisense-SWNT solutions in water and eluting free RNA (hybridized).

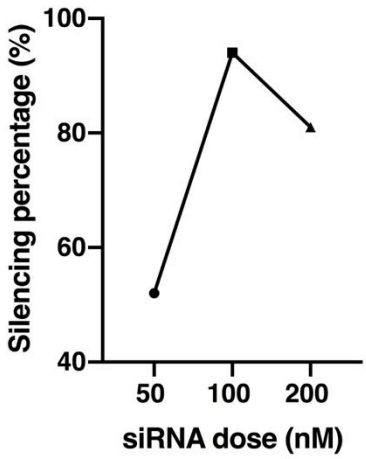

Supplementary Fig. 7. Optimization of siRNA dose on SWNTs for *mGFP5* silencing. Final siRNA concentration of 50, 100 and 200 nM on SWNTs, and corresponding gene silencing efficiencies at 1-day post-infiltration measured via qPCR.

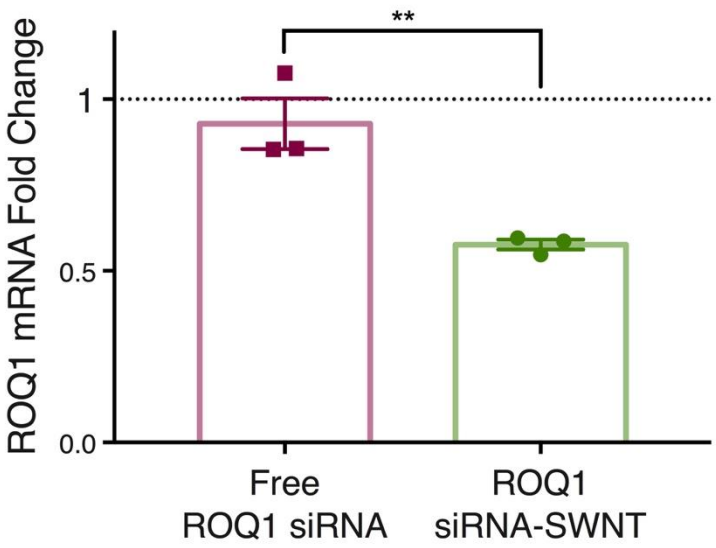

Supplementary Fig. 8. Silencing of endogenous functional *Nicotiana benthamiana* ROQ1 gene with siRNA-SWNTs. Free ROQ1 siRNA without SWNTs do not show significant silencing of ROQ1 gene, whereas 100 nM ROQ1 siRNA on SWNTs yields nearly 50% mRNA reduction at Day 1 as assessed by qPCR of infiltrated *Nicotiana benthamiana* leaves compared to the non-treated control leaves. ** P = 0.0094 in two-tailed t-test. Error bars indicate s.e.m. (n = 3).

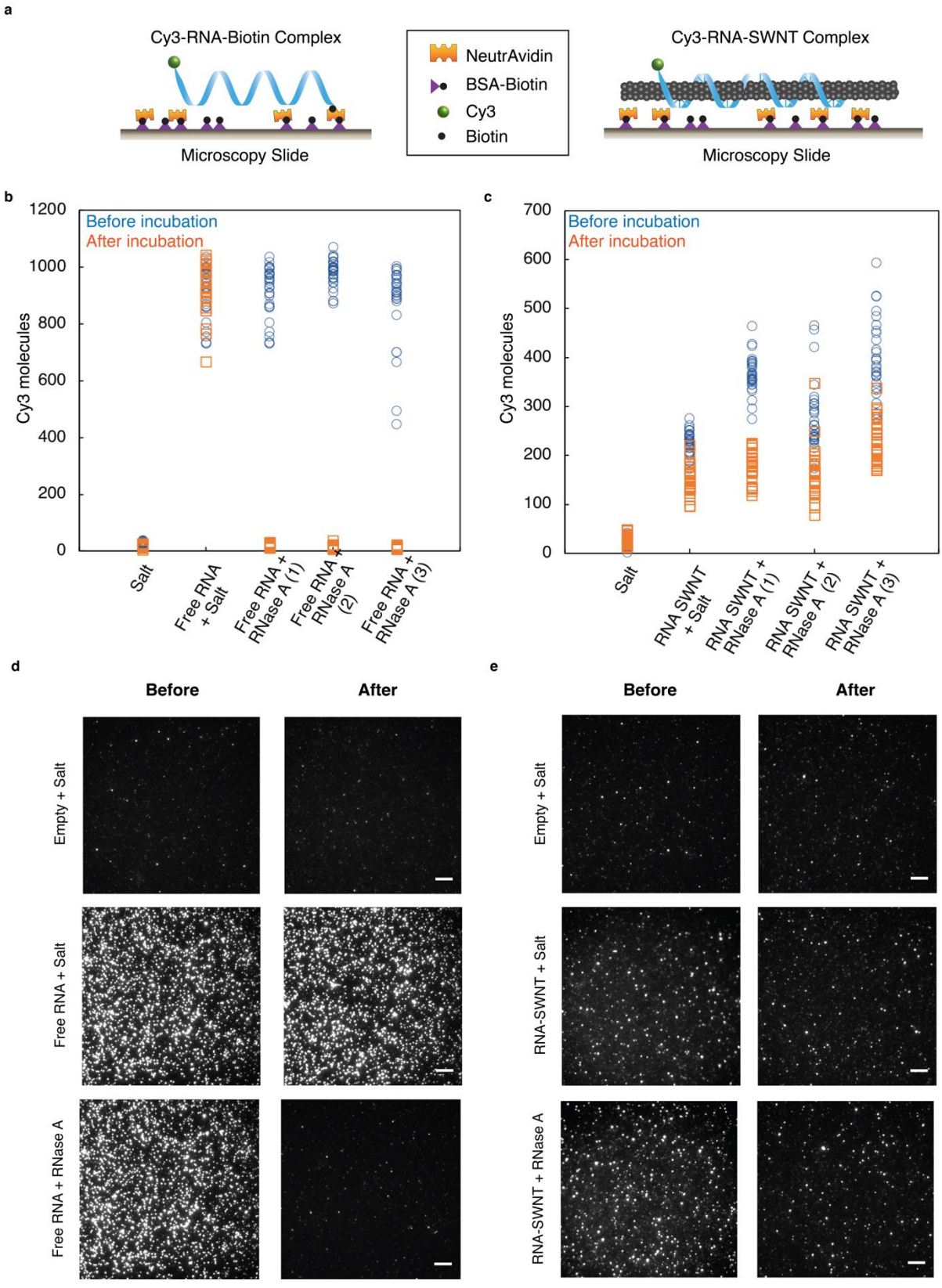
a
Cy3-RNA-Biotin Complex
Microscopy Slide
NeutrAvidin
BSA-Biotin
Cy3
Biotin
Cy3-RNA-SWNT Complex
Microscopy Slide
b
Before incubation
After incubation
Cy3 molecules
1200
1000
800
600
400
200
0
Salt
Free RNA + Salt
Free RNA + RNase A (1)
Free RNA + RNase A (2)
Free RNA + RNase A (3)
c
Before incubation
After incubation
Cy3 molecules
700
600
500
400
300
200
100
0
Salt
RNA SWNT + Salt
RNA SWNT + RNase A (1)
RNA SWNT + RNase A (2)
RNA SWNT + RNase A (3)
d
Before
After
Empty + Salt
Free RNA + Salt
Free RNA + RNase A
e
Before
After
Empty + Salt
RNA-SWNT + Salt
RNA-SWNT + RNase A

Supplementary Fig. 9. Single molecule total internal reflection fluorescence (smTIRF) microscopy demonstrates RNA protection from nuclease degradation when adsorbed to SWNTs. a Schematics of microfluidic slides for immobilization and smTIRF imaging of Cy3-RNA-Biotin and Cy3-RNA-SWNT complexes. **b** Raw smTIRF data for empty channel rinsed with salt solution, free RNA incubated with salt solution, and three experimental replicates of free RNA incubated with RNase A, blue: before incubation and orange: after incubation. Data from 30 fields of views was plotted for each sample before and after treatment. **c** Raw smTIRF data for empty channel rinsed with salt solution, RNA-SWNT incubated with salt solution, and three experimental replicates of RNA-SWNT incubated with RNase A, blue: before incubation and orange: after incubation with RNase A. Data from 30 fields of views was plotted for each sample before and after treatment. **d** Representative TIRF microscopy images for each sample of free RNA before and after incubation with salt and RNase A. **e** Representative TIRF microscopy images for each sample of RNA-SWNTs before and after incubation with salt and RNase A. All scale bars, 5 μm.

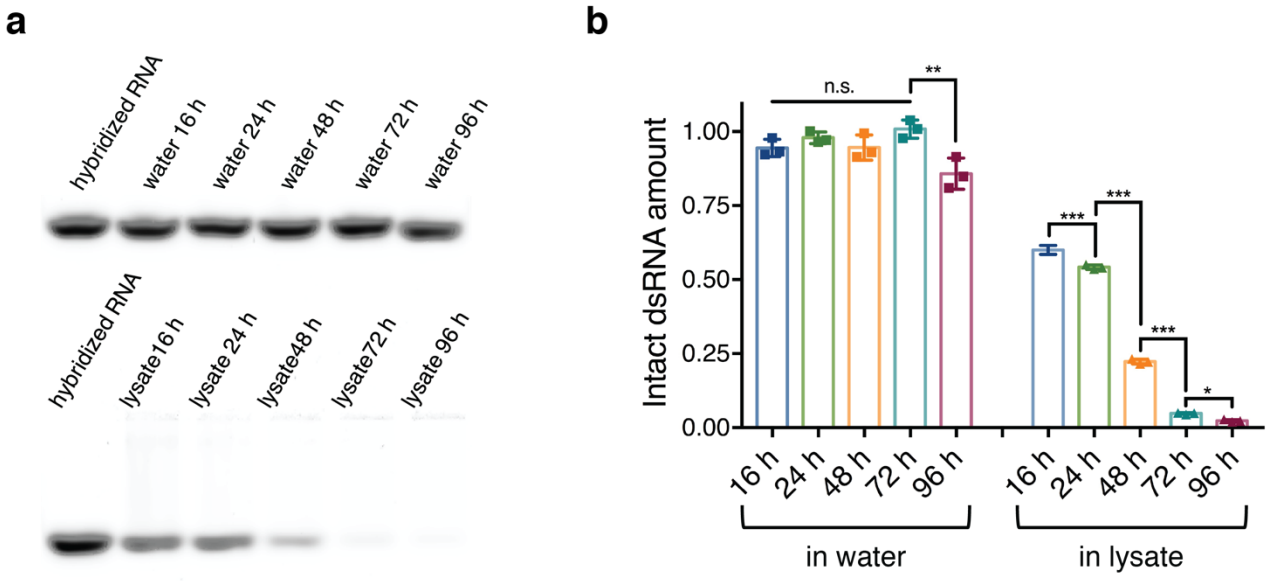

Supplementary Fig. 10. dsRNA stability in cell lysate. a Hybridized double stranded siRNA samples incubated in nuclease-free water and cell lysate solutions at room temperature for 16, 24, 48, 72 and 96 hours, and run on a 2% agarose gel. **b** Quantification of RNA bands from the gel in part a and two other replicates, using the Image J gel analyzer tool. All band intensities are normalized with respect to the hybridized RNA band intensity at time zero without any treatment.

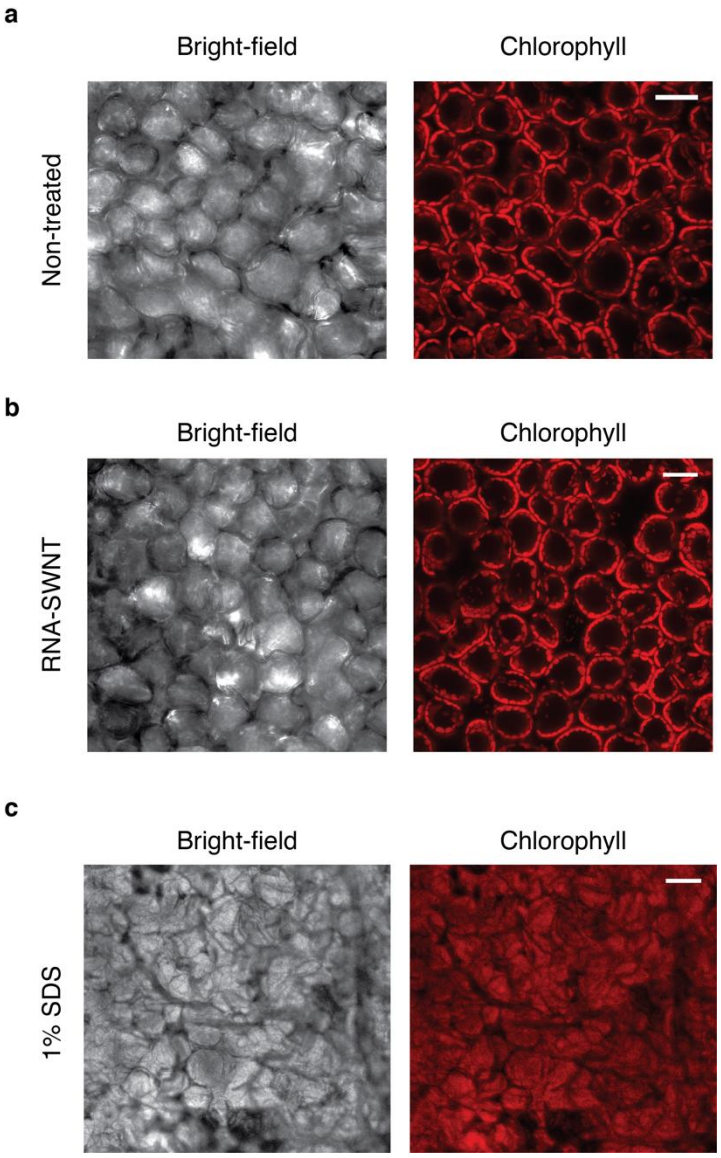

Supplementary Fig. 11. Confocal microscopy imaging of the *Nb* leaf tissue to assess cellular damage. a Representative bright-field and chlorophyll images of non-treated *Nb* leaf. **b** RNA-SWNT treated *Nb* leaf and **c** 1% SDS treated *Nb* leaf as a positive control of leaf tissue damage. All scale bars, 20 µm.

Supplementary Table 3: RNA sequences and primers used in this study

RNA sequences:	(all sequences written as 5' to 3')
a-antisense	UUC CGU AUG UUG CAU CAC CTT
a-sense	GGU GAU GCA ACA UAC GGA ATT
b-antisense	GGG UGA AGG UGA UGC AAC ATT
b-sense	UGU UGC AUC ACC UUC ACC CTT
s-antisense	GUA UCU CUU CAU AGC CUU ATT
s-sense	UAA GGC UAU GAA GAG AUA CTT
Cy3 tagged a-antisense	Cy3/UUC CGU AUG UUG CAU CAC CTT
ROQ1-sense	GGU UUA AUU UGG UGU AUA A
ROQ1-antisense	UUA UAC ACC AAA UUA AAC C
Primers for qPCR:	
EF1 forward	TGG TGT CCT CAA GCC TGG TAT GGT TG
EF1 reverse	ACG CTT GAG ATC CTT AAC CGC AAC ATT CTT
mGFP5 forward	AGT GGA GAG GGT GAA GGT GAT G
mGFP5 reverse	GCA TTG AAC ACC ATA AGA GAA AGT AGT G
NbrbohB forward	TTT CTC TGA GGT TTG CCA GCC ACC ACC TAA
NbrbohB reverse	GCC TTC ATG TTG TTG ACA ATG TCT TTA ACA
ROQ1 forward	TCC CCG ACA TAA AGG AAT GC
ROQ1 reverse	GTC CCC TGG ACT CAA ACA GG

REFERENCES AND NOTES

1. W. Lau, E. S. Sattely, Six enzymes from mayapple that complete the biosynthetic pathway to the etoposide aglycone. *Science* **349**, 1224–1228 (2015).

2. J. M. Casacuberta, Y. Devos, P. du Jardin, M. Ramon, H. Vaucheret, F. Nogué, Biotechnological uses of RNAi in plants: Risk assessment considerations. *Trends Biotechnol.* **33**, 145–147 (2015).

3. N. Dhaka, R. Sharma, MicroRNAs as targets for engineering biofuel feedstock Sorghum. *Indian J. Plant Physiol.* **22**, 484–492 (2017).

4. S. C. Sukenik, K. Karuppanan, Q. Li, C. B. Lebrilla, S. Nandi, K. A. McDonald, Transient recombinant protein production in glycoengineered *Nicotiana benthamiana* cell suspension culture. *Int. J. Mol. Sci.* **19**, 1205 (2018).

5. I. Small, RNAi for revealing and engineering plant gene functions. *Curr. Opin. Biotechnol.* **18**, 148–153 (2007).

6. C.-G. Duan, C.-H. Wang, H.-S. Guo, Application of RNA silencing to plant disease resistance. *Silence* **3**, 5 (2012).

7. F. Schwab, G. Zhai, M. Kern, A. Turner, J. L. Schnoor, M. R. Wiesner, Barriers, pathways and processes for uptake, translocation and accumulation of nanomaterials in plants—Critical review. *Nanotoxicology* **10**, 257–278 (2016).

8. A. T. Silva, A. Nguyen, C. Ye, J. Verchot, J. H. Moon, Conjugated polymer nanoparticles for effective siRNA delivery to tobacco BY-2 protoplasts. *BMC Plant Biol.* **10**, 291 (2010).

9. T. M. Burch-Smith, J. C. Anderson, G. B. Martin, S. P. Dinesh-Kumar, Applications and advantages of virus-induced gene silencing for gene function studies in plants. *Plant J.* **39**, 734–746 (2004).

10. A. Anand, T. J. Jones, in *Agrobacterium Biology: From Basic Science to Biotechnology*, S. B. Gelvin, Ed. (Springer International Publishing, 2018), pp. 489–507.

11. N. J. Baltes, J. Gil-Humanes, D. F. Voytas, Genome engineering and agriculture: Opportunities and challenges, in *Progress in Molecular Biology and Translational Science* (Academic Press, 2018).

12. G. S. Demirer, M. P. Landry, Delivering genes to plants. *Chem. Eng. Prog.* **113**, 40–45 (2017).

13. F.-P. Chang, L.-Y. Kuang, C.-A. Huang, W.-N. Jane, Y. Hung, Y. C. Hsing, C.-Y. Mou, A simple plant gene delivery system using mesoporous silica nanoparticles as carriers. *J. Mater. Chem. B* **1**, 5279–5287 (2013).

14. H. I. Hussain, Z. Yi, J. E. Rookes, L. X. Kong, D. M. Cahill, Mesoporous silica nanoparticles as a biomolecule delivery vehicle in plants. *J. Nanopart. Res.* **15**, 1676 (2013).

15. S. Martin-Ortigosa, J. S. Valenstein, W. Sun, L. Moeller, N. Fang, B. G. Trewyn, V. S.-Y. Lin, K. Wang, Parameters affecting the efficient delivery of mesoporous silica nanoparticle materials and gold nanorods into plant tissues by the biolistic method. *Small* **8**, 413–422 (2012).

16. G. S. Demirer, H. Zhang, J. L. Matos, N. S. Goh, F. J. Cunningham, Y. Sung, R. Chang, A. J. Aditham, L. Chio, M.-J. Cho, B. Staskawicz, M. P. Landry, High aspect ratio nanomaterials enable delivery of functional genetic material without DNA integration in mature plants. *Nat. Nanotechnol.* **14**, 456–464 (2019).

17. S.-Y. Kwak, T. T. Salim Lew, C. J. Sweeney, V. B. Koman, M. H. Wong, K. Bohmert-Tatarev, K. D. Snell, J. S. Seo, N.-H. Chua, M. S. Strano, Chloroplast-selective gene delivery and expression in planta using chitosan-complexed single-walled carbon nanotube carriers. *Nat. Nanotechnol.* **14**, 447–455 (2019).

8. S. Martin-Ortigosa, D. J. Peterson, J. S. Valenstein, V. S.-Y. Lin, B. G. Trewyn, L. A. Lyznik, K. Wang, Mesoporous silica nanoparticle-mediated intracellular Cre protein delivery for maize genome editing via *loxP* site excision. *Plant Physiol.* **164**, 537–547 (2014).

19. N. Mitter, E. A. Worrall, K. E. Robinson, P. Li, R. G. Jain, C. Taochy, S. J. Fletcher, B. J. Carroll, G. Q. Lu, Z. P. Xu, Clay nanosheets for topical delivery of RNAi for sustained protection against plant viruses. *Nat. Plants* **3**, 16207 (2017).

0. M. H. Wong, R. P. Misra, J. P. Giraldo, S.-Y. Kwak, Y. Son, M. P. Landry, J. W. Swan, D. Blankschtein, M. S. Strano, Lipid exchange envelope penetration (LEEP) of nanoparticles for plant engineering: A universal localization mechanism. *Nano Lett.* **16**, 1161–1172 (2016).

1. J. P. Giraldo, M. P. Landry, S. M. Faltermeier, T. P. McNicholas, N. M. Iverson, A. A. Boghossian, N. F. Reuel, A. J. Hilmer, F. Sen, J. A. Brew, M. S. Strano, Plant nanobionics approach to augment photosynthesis and biochemical sensing. *Nat. Mater.* **13**, 400–408 (2014).

22. Y. Wu, J. A. Phillips, H. Liu, R. Yang, W. Tan, Carbon nanotubes protect DNA strands during cellular delivery. *ACS Nano* **2**, 2023–2028 (2008).

23. H. Wang, G. I. Koleilat, P. Liu, G. Jiménez-Osés, Y.-C. Lai, M. Vosgueritchian, Y. Fang, S. Park, K. N. Houk, Z. Bao, High-yield sorting of small-diameter carbon nanotubes for solar cells and transistors. *ACS Nano* **8**, 2609–2617 (2014).

24. Q. Liu, B. Chen, Q. Wang, X. Shi, Z. Xiao, J. Lin, X. Fang, Carbon nanotubes as molecular transporters for walled plant cells. *Nano Lett.* **9**, 1007–1010 (2009).

25. M. F. Serag, N. Kaji, C. Gaillard, Y. Okamoto, K. Terasaka, M. Jabasini, M. Tokeshi, H. Mizukami, A. Bianco, Y. Baba, Trafficking and subcellular localization of multiwalled carbon nanotubes in plant cells. *ACS Nano* **5**, 493–499 (2011).

26. M. H. Wong, J. P. Giraldo, S.Y. Kwak, V. B. Koman, R. Sinclair, T. T. S. Lew, G. Bisker, P. Liu, M. S. Strano, Nitroaromatic detection and infrared communication from wild-type plants using plant nanobionics. *Nat. Mater.* **16**, 264–272 (2017).

27. P. Wang, E. Lombi, F.-J. Zhao, P. M. Kopittke, Nanotechnology: A new opportunity in plant sciences. *Trends Plant Sci.* **21**, 699–712 (2016).

28. R. Nair, S. H. Varghese, B. G. Nair, T. Maekawa, Y. Yoshida, D. S. Kumar, Nanoparticulate material delivery to plants. *Plant Sci.* **179**, 154–163 (2010).

29. M. Khodakovskaya, E. Dervishi, M. Mahmood, Y. Xu, Z. Li, F. Watanabe, A. S. Biris, Carbon nanotubes are able to penetrate plant seed coat and dramatically affect seed germination and plant growth. *ACS Nano* **3**, 3221–3227 (2009).

30. K. Kalantidis, M. Tsagris, M. Tabler, Spontaneous short-range silencing of a GFP transgene in *Nicotiana benthamiana* is possibly mediated by small quantities of siRNA that do not trigger systemic silencing. *Plant J.* **45**, 1006–1016 (2006).

31. G. Agaësse, L. Barbollat-Boutrand, M. El Kharbili, O. Berthier-Vergnes, I. Masse, p53 targets TSPAN8 to prevent invasion in melanoma cells. *Oncogenesis* **6**, e309 (2017).

32. T. Shimada, J. Takagi, T. Ichino, M. Shirakawa, I. Hara-Nishimura, Plant vacuoles. *Annu. Rev. Plant Biol.* **69**, 123–145 (2018).

33. J. H. Choi, M. S. Strano, Solvatochromism in single-walled carbon nanotubes. *Appl. Phys. Lett.* **90**, 223114 (2007).

34. T. V. Galassi, P. V. Jena, J. Shah, G. Ao, E. Molitor, Y. Bram, A. Frankel, J. Park, J. Jessurun, D. S. Ory, A. Haimovitz-Friedman, D. Roxbury, J. Mittal, M. Zheng, R. E. Schwartz, D. A. Heller, An optical nanoreporter of endolysosomal lipid accumulation reveals enduring effects of diet on hepatic macrophages in vivo. **10**, eaar2680 (2018).

5. R. M. Williams, C. Lee, T. V. Galassi, J. D. Harvey, R. Leicher, M. Sirenko, M. A. Dorso, J. Shah, N. Olvera, F. Dao, D. A. Levine, D. A. Heller, Noninvasive ovarian cancer biomarker detection via an optical nanosensor implant. *Sci. Adv.* **4**, eaaq1090 (2018).

36. D. W. Bartlett, M. E. Davis, Insights into the kinetics of siRNA-mediated gene silencing from live-cell and live-animal bioluminescent imaging. *Nucleic Acids Res.* **34**, 322–333 (2006).

37. A. Schultink, T. Qi, A. Lee, A. D. Steinbrenner, B. Staskawicz, Roq1 mediates recognition of the Xanthomonas and Pseudomonas effector proteins XopQ and HopQ1. *Plant J.* **92**, 787–795 (2017).

8. H. Yoshioka, N. Numata, K. Nakajima, S. Katou, K. Kawakita, O. Rowland, J. D. G. Jones, N. Doke, *Nicotiana benthamiana* gp91^{phox} homologs *NbrbohA* and *NbrbohB* participate in H_2O_2 accumulation and resistance to *Phytophthora infestans*. *Plant Cell* **15**, 706–718 (2003).

39. H. Yuan, S. Hu, P. Huang, H. Song, K. Wang, J. Ruan, R. He, D. Cui, Single walled carbon nanotubes exhibit dual-phase regulation to exposed Arabidopsis mesophyll cells. *Nanoscale Res. Lett.* **6**, 44 (2011).

40. C. M. Goodman, C. D. McCusker, T. Yilmaz, V. M. Rotello, Toxicity of gold nanoparticles functionalized with cationic and anionic side chains. *Bioconjug. Chem.* **15**, 897–900 (2004).

41. Y. Qi, Y. Zhang, F. Zhang, J. A. Baller, S. C. Cleland, Y. Ryu, C. G. Starker, D. F. Voytas, Increasing frequencies of site-specific mutagenesis and gene targeting in *Arabidopsis* by manipulating DNA repair pathways. *Genome Res.* **23**, 547–554 (2013).

42. J. T. Del Bonis-O'Donnell, A. Beyene, L. Chio, G. Demirer, D. Yang, M. P. Landry, Engineering molecular recognition with bio-mimetic polymers on single walled carbon nanotubes. *J. Vis. Exp.* **2017**, e55030 (2017).

43. A. G. Beyene, G. S. Demirer, M. P. Landry, Nanoparticle-templated molecular recognition platforms for detection of biological analytes. *Curr. Protoc Chem. Biol.* **8**, 197–223 (2016).

44. T. D. Schmittgen, K. J. Livak, Analyzing real-time PCR data by the comparative C_T method. *Nat. Protoc.* **3**, 1101–1108 (2008).

45. S. Kruss, M. P. Landry, E. Vander Ende, B. M. A. Lima, N. F. Reuel, J. Zhang, J. Nelson, B. Mu, A. Hilmer, M. Strano, Neurotransmitter detection using corona phase molecular recognition on fluorescent single-walled carbon nanotube sensors. *J. Am. Chem. Soc.* **136**, 713–724 (2014).

46. W. Tang, V. Samuels, N. Whitley, N. Bloom, T. DeLaGarza, R. J. Newton, Post-transcriptional gene silencing induced by short interfering RNAs in cultured transgenic plant cells. *Genomics Proteomics Bioinformatics* **2**, 97–108 (2004).

47. R. R. Johnson, A. T. C. Johnson, M. L. Klein, Probing the structure of DNA−carbon nanotube hybrids with molecular dynamics. *Nano Lett.* **8**, 69–75 (2008).

48. A. Das, A. K. Sood, P. K. Maiti, M. Das, Binding of nucleobases with single-walled carbon nanotubes: Theory and experiment. *Chem. Phys. Lett.* **453**, 266–273 (2008).

49. C. Salvador-Morales, E. Flahaut, E. Sim, J. Sloan, M. L. H. Green, R. B. Sim, Complement activation and protein adsorption by carbon nanotubes. *Mol. Immunol.* **43**, 193–201 (2006).

50. J. D. Harvey, P. V. Jena, H. A. Baker, G. H. Zerze, R. M. Williams, T. V. Galassi, D. Roxbury, J. Mittal, D. A. Heller, A carbon nanotube reporter of microRNA hybridization events in vivo. *Nat. Biomed. Eng.* **1**, 0041 (2017).

51. R. L. Pinals, D. Yang, A. Lui, W. Cao, M. P. Landry, Corona exchange dynamics on carbon nanotubes by multiplexed fluorescence monitoring. *J. Am. Chem. Soc.* **142**, 1254–1264 (2020).

52. J.-W. Shen, T. Wu, Q. Wang, Y. Kang, Induced stepwise conformational change of human serum albumin on carbon nanotube surfaces. *Biomaterials* **29**, 3847–3855 (2008).

53. Z. Yang, Z. Wang, X. Tian, P. Xiu, R. Zhou, Amino acid analogues bind to carbon nanotube via π-π interactions: Comparison of molecular mechanical and quantum mechanical calculations. *J. Chem. Phys.* **136**, 025103 (2012).

54. C. Rajesh, C. Majumder, H. Mizuseki, Y. Kawazoe, A theoretical study on the interaction of aromatic amino acids with graphene and single walled carbon nanotube. *J. Chem. Phys.* **130**, 124911 (2009).

55. A. G. Beyene, A. A. Alizadehmojarad, G. Dorlhiac, N. Goh, A. M. Streets, P. Král, L. Vuković, M. P. Landry Ultralarge modulation of fluorescence by neuromodulators in carbon nanotubes functionalized with self-assembled oligonucleotide rings. *Nano Lett.* **18**, 6995–7003 (2018).

56. J. Kuriyan, B. Konforti, D. Wemmer, *The Molecules of Life: Physical and Chemical Principles* (Garland Science, 2012).

57. N. Lu, Y. Sui, Y. Ding, R. Tian, L. Li, F. Liu, Adsorption of human serum albumin on functionalized single-walled carbon nanotubes reduced cytotoxicity. *Chem. Biol. Interact.* **295**, 64–72 (2018).

58. L. Brocchieri, S. Karlin, Protein length in eukaryotic and prokaryotic proteomes. *Nucleic Acids Res.* **33**, 3390–3400 (2005).